Structure Function Analysis of Water Vapor Simulated with a Convection-Permitting Model and Comparison to Airborne Lidar Observations

TOBIAS SELZ, LUCAS FISCHER, AND GEORGE C. CRAIG

Meteorologisches Institut, Ludwig-Maximilians-Universität München, München, Germany

(Manuscript received 27 May 2016, in final form 2 January 2017)

ABSTRACT

The spatial scale dependence of midlatitude water vapor variability in the high-resolution limited-area model COSMO is evaluated using diagnostics of scaling behavior. Past analysis of airborne lidar measurements showed that structure function scaling exponents depend on the corresponding airmass characteristics, and that a classification of the troposphere into convective and nonconvective layers led to significantly different power-law behaviors for each of these two regimes. In particular, scaling properties in the convective air mass were characterized by rough and highly intermittent data series, whereas the nonconvective regime was dominated by smoother structures with weaker small-scale variability. This study finds similar results in a model simulation with an even more pronounced distinction between the two air masses. Quantitative scaling diagnostics agree well with measurements in the nonconvective air mass, whereas in the convective air mass the simulation shows a much higher intermittency. Sensitivity analyses were performed using the model data to assess the impact of limitations of the observational dataset, which indicate that analyses of lidar data most likely underestimated the intermittency in convective air masses due to the small samples from single flight tracks, which led to a bias when data with poor fits were rejected. Though the quantitative estimation of intermittency remains uncertain for convective air masses, the ability of the model to capture the dominant weather regime dependence of water vapor scaling properties is encouraging.

1. Introduction

The complex interaction of water vapor with atmospheric motion and mixing processes over a wide range of spatial scales, together with various sinks and sources, leads to a very heterogeneous humidity distribution in the troposphere. A better understanding of the spatial variability of water vapor in the free troposphere is essential for the representation of clouds, including fractional cloud cover, in numerical weather prediction models (NWP) and global circulation models (GCM) (e.g., Stevens and Bony 2013a). Cloud properties are strongly dependent on the humidity distribution of the ambient air, which in nature varies significantly over distances corresponding to the size of a model grid box (Cusack et al. 1999; Tompkins 2002; Wang et al. 2010). Due to the fact that clouds reflect solar radiation back to space and trap infrared radiation emitted by the surface, even small differences in modeling cloud feedbacks can have a strong influence on climate simulations (e.g., Yokohata et al. 2005; Zhang 2013).

In weather and climate models the parameterizations of cloud processes strongly depend on the assumptions made about the subgrid-scale variability of water vapor. Thus, a precise characterization of the small-scale tropospheric water vapor variability based on observations or at least a sound knowledge of the variability-forming processes is required. Yet observational studies are scarce, and the coupling processes between water vapor and the atmospheric flow are still insufficiently investigated (Stevens and Bony 2013b). The interaction of water vapor as an active scalar within the atmospheric flow leads to a complex scale dependence that is relevant for the subgrid-scale representation of moist processes in models (Pressel and Collins 2012). Future weather and climate model parameterizations should ideally be able to represent the scale dependence in the tropospheric humidity field consistently over a range of spatial scales down to cloud-resolving scales or even smaller (Schemann et al. 2013).

A well-established method for representing and quantifying scale dependence in the observed tropospheric water vapor field is the calculation of horizontal structure functions of different orders (Cho et al. 1999, 2000;

Corresponding author e-mail: Tobias Selz, tobias.selz@lmu.de

DOI: 10.1175/JAS-D-16-0160.1

Fischer et al. 2012, 2013; Lovejoy et al. 2010; Pressel and Collins 2012). Over certain ranges of spatial scales, a power-law behavior has been found that allows for the determination of the power-law exponent, also called the scaling exponent, as a measure of spatial variability.

It has been shown by observational and modeling studies that passive scalars in strongly stratified turbulence exhibit a similar spatial scaling in the inertial range as in three-dimensional turbulence (i.e., a $\beta = -5/3$ Fourier power law or, equivalently, a $\zeta_2 = 2/3$ second-order structure function exponent) (e.g., Brethouwer and Lindborg 2008). However, recent observational studies of water vapor fluctuations in the middle and lower troposphere deviate from this expectation, both on spatial scales smaller than 100 km (Cho et al. 1999, 2000; Lovejoy et al. 2010; Fischer et al. 2012, 2013; Pressel et al. 2010, 2014) and on larger scales (Kahn and Teixeira 2009; Kahn et al. 2011; Pressel and Collins 2012). Several explanations have been discussed in the literature for these different scaling exponents. They include universality assumptions based on the theory of a passive tracer (Nastrom et al. 1986; Cho et al. 1999), increasing exponents with height (Tjemkes and Visser 1994; Kahn et al. 2011), boundary layer versus free troposphere (Cho et al. 2000; Pressel and Collins 2012), and anisotropic scaling (Lovejoy et al. 2010).

The implications of the different observed exponents for the existence of universal power laws are not clear, since the data used in each case are limited, and the results may not be comparable. It is, however, interesting to consider whether distinct physical mechanisms may be dominant in different regions. Some insight has been obtained from height-resolved airborne lidar measurements that show a distinction between the scaling behavior found in air masses dominated by small-scale convective events and in air masses dominated by large-scale advection processes (Fischer et al. 2012, 2013). The second-order structure function exponents were found to vary around $\zeta_2 = 1.2$ in nonconvective air masses and with a much flatter spectrum of around $\zeta_2 = 2/3$ in convectively influenced air masses (Fischer et al. 2013). It was suggested that the water vapor distribution is determined in nonconvective regions by a downscale cascade of variance by advective mixing but is increasingly influenced in convective regions by local injection of humidity by moist updrafts. However, the processes remain unclear, since the exponent in the nonconvective region is not consistent with the 2/3 value expected for a passive tracer in homogeneous stratified turbulence.

Even though the interactions of dynamics and moisture in the atmosphere are not fully understood, the observations of power-law scaling allow for a reality check of NWP models and GCMs concerning water vapor variability (Kahn et al. 2011). While this is not a traditional validation measure, a model's ability to reproduce the observed scale dependence behavior provides a statistical measure of the accuracy of its moist dynamics and physics (Skamarock 2004). In other words, if a model does not reproduce the real atmosphere's scale-dependence behavior appropriately, shortcomings in the numerics or parameterizations are likely.

In the case of kinetic energy, the evaluation of scaling exponents has provided valuable insights into model performance (Skamarock 2004; Hamilton et al. 2008; Bierdel et al. 2012; Fang and Kuo 2015). For water vapor, Schemann et al. (2013) investigated the scaling behaviors of a GCM, an NWP model, and a large-eddy simulation (LES) and the implication for cloud parameterizations. They found Fourier power-law exponents of around $\beta = -2$ for scales ranging from global down to cloud resolving. However their main intention was to show the universality of power-law scaling over a wide range of scales, and they did not investigate the variations in scaling behavior with respect to height, latitude, or different meteorological conditions that the observations show. The study of Kahn et al. (2011) appears to be unique in its use of observational benchmarks of water vapor scaling exponents for the evaluation of global NWP and climate models. Using AIRS data, they showed that the spectral slopes on horizontal scales from 150 up to 1000 km of global NWP and climate models are generally too steep: The models tend to underestimate small-scale variance of water vapor in comparison to observations. It was argued by Fischer et al. (2013) that the flatter spectra were associated with air masses influenced by cumulus convection, a process which is not resolved in the global NWP and climate models investigated by Kahn et al. (2011).

In the present study, we will thus consider a regional NWP model with a horizontal resolution of a few kilometers that can simulate convective clouds without requiring a parameterization for deep convection. After giving an overview of the model setup and the structure function method we use in section 2, this paper will address two basic questions. The first goal is to investigate if the different scaling behavior of water vapor found in Fischer et al. (2012) and Fischer et al. (2013) between a convecting air mass and a nonconvecting air mass can be reproduced by such a high-resolution model (section 3a). The second aim is then to use the model output as a surrogate dataset to assess the consequences of certain limitations of the observations, such as flight length, data

gaps caused by optically thick clouds, and the small samples of a single flight track (section 3b).

2. Data and method

a. COSMO simulation details

The Consortium for Small-Scale Modeling (COSMO) model is the current limited-area numerical weather prediction model of the German Weather Service (DWD) for operational short-range weather forecasts (Baldauf et al. 2011). The operational spatial resolution of 2.8 km is used in our simulations, in which deep moist convection and the associated feedback mechanisms to the larger scales of motion are considered to be explicitly resolved. Shallow convection (nonprecipitating, depth less than 250 hPa) is still parameterized with the Tiedtke scheme (Tiedtke 1989). Precipitation processes are explicitly described using a bulk cloud microphysical scheme. For parameterization of cloud cover, the COSMO model uses a relative humidity–based formulation in the radiation scheme, while a probability density function (PDF)-based scheme within the turbulence model is used to parameterize boundary layer clouds. The simulations analyzed in this paper therefore resolve only deep convective motions, and the small-scale humidity distribution is still influenced by parameterizations similar to coarser numerical models. This is likely to impair the simulation quality on scales close to the model resolution.

In the vertical, the COSMO model in our setup uses a modified, height-based Gal-Chen coordinate system, consisting of 50 irregularly distributed layers from 10 m above ground level up to 21 500 m above sea level. The model levels are terrain following in the lower levels but continuously changing to levels of constant height in the upper troposphere. Since the analyzed data series in this study are only taken over flat terrain, we consider the model levels as being constant in (sea level) height. Further justification for this assumption is provided by Skamarock (2004), who found no significant impact for spectral analysis if constant model, pressure, or height surfaces were used.

The simulation was performed on a large domain, covering all of Europe and parts of the North Atlantic, and simulated the weather development from 19 to 23 July 2007, a period with an almost stationary low pressure system over Great Britain with southwesterly flow and heavy and strongly forced convection over central Europe. This experiment served as the control experiment for the predictability study of Selz and Craig (2015), and we refer to this text for further details. For the present investigation, we only use data valid at 1400 UT 20 July 2007 and on a small subdomain (see below).

b. Structure function methodology

In general, the structure function of order q of a one-dimensional field $f(x)$ is defined by

$$S_q(r) = \langle |f(x+r) - f(x)|^q \rangle , \tag{1}$$

where the angle brackets denote an ensemble average over different realizations of the field f (Pressel and Collins 2012). The difference $f(x+r) - f(x)$ is called an increment of f at distance or separation r, and hence the structure functions describe the moments of the increment's PDF. In practice, one usually assumes homogeneity over a certain range, and the ensemble mean is replaced by an arithmetic mean over spatially displaced increments:

$$S_q(r) = \frac{1}{N} \sum_i |f(x_i + r) - f(x_i)|^q , \tag{2}$$

where N is the number of included points x_i. If a three-dimensional atmospheric field $f(x, y, z)$ is considered, it is often also possible to assume homogeneity over a volume and extend the arithmetic mean further by considering displacements in the y and/or the z direction as well:

$$S_q(r) = \frac{1}{N} \sum_{i,j,k} |f(x_i + r, y_j, z_k) - f(x_i, y_j, z_k)|^q , \tag{3}$$

with N the total number of points considered. Note that the separation r is still only applied in the x direction, and (3) is not a full three-dimensional generalization of (1), which would require an assumption of isotropy. When gridded data from model output or sampled observations are considered, the indices i, j, and k refer to grid points, and the separation r is an integer multiplicative of the grid spacing Δx.

The dependence of the structure function on the distance r is often found to follow a power law, represented by the relation

$$S_q(r) \propto r^{\zeta_q}, \tag{4}$$

where ζ_q are called scaling exponents of order q. Thus, given a structure function of order q, the scaling exponent ζ_q can be determined by fitting a straight line to the double-logarithmic S_q–r diagram. The power-law scaling regime and thus the r interval used for the fit is usually restricted on both sides (e.g., by the resolution at small scales and by domain size at large scales). For the

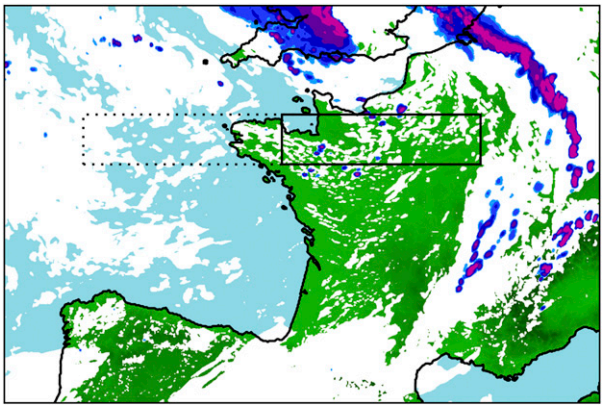

FIG. 1. Simulated weather situation over western Europe at 1400 UT 20 July 2007. Dark blue to red colors show increasing precipitation rate, and white indicates cloud cover exceeding 50%. Green and light blue colors denote land and sea surface, respectively. The solid box indicates the domain of structure function analysis. The dashed box shows an extended domain, which is considered in section 3b(1) only.

analysis of model output in this paper, displacements smaller than 11 km or 4 times the grid length are not considered because they are below the effective resolution of the model and suffer from numerical diffusion (Bierdel et al. 2012). An upper bound displacement range of 100 km was chosen, which equals about one-fifth of the domain size in the x direction.

The scaling exponent of the first-order structure function ζ_1, often called the Hurst exponent H or "smoothness," characterizes the nonstationarity of the data (Marshak et al. 1997) (i.e., there is significant variability on scales larger than those sampled). It can be used to quantify power-law scaling and to characterize the spatial correlative structure of an atmospheric field (Pressel and Collins 2012). The range of H is from 0 to 1, with values near 0 characterizing rough, nearly stationary signals and values near 1 characterizing smooth, nonstationary signals (Tuck et al. 2003).

The second-order structure function exponent ζ_2 is well known because of its duality with the Fourier power spectrum. Under the assumption that power-law scaling is satisfied for all encompassed scales, a simple relation holds between the scaling exponent of the second-order structure function ζ_2 and the slope β in the double-logarithmic representation of the Fourier spectrum (Lewis et al. 2004):

$$\zeta_2 = -\beta - 1. \tag{5}$$

The scaling exponents ζ_q are usually not independent from each other: for ordinary or nonintermittent scaling ζ_q is proportional to the order q. Intermittency is, however, characterized by large jumps and sharp gradients in the field $f(x)$, which flares out the tails of the increment PDFs with decreasing separation r, making large fluctuations over short distances more likely (Shraiman and Siggia 2000). Since higher-order scaling exponents give more weight to these tails, the scaling exponents ζ_q decrease with increasing order q compared to the nonintermittent behavior. Note that we use the term intermittency in the sense of Calif and Schmitt (2012), who define intermittency as the property of having large fluctuations at all scales, with a correlated structure.

To quantify the intermittency of a data series, Pierrehumbert (1996) suggested the following relationship between the scaling exponents and the order q:

$$\zeta_q = \frac{aq}{1 + aq/\zeta_\infty}, \tag{6}$$

where $1/\zeta_\infty \geq 0$ denotes the intermittency parameter. For ordinary scaling, $1/\zeta_\infty = 0$, and the linear relation is retained. A higher value of $1/\zeta_\infty$ indicates a greater departure of the scaling exponents from ordinary scaling and thus a higher intermittency. To determine $1/\zeta_\infty$ in our study, we applied nonlinear curve fitting to the first five scaling exponents ζ_q, with consideration of their estimated standard deviation σ_q from the linear regression. An illustration of the scaling exponent and intermittency determination is given (see Fig. 5) and will be discussed in detail later.

3. Results

a. *Scaling exponents and intermittency of simulated water vapor*

In this section, we investigate the scaling properties of simulated water vapor fields with the structure function methodology described above. In particular, we look for power-law scaling in the water vapor field at different heights over a region of shallow cumulus convection. Earlier results from observational data suggested scaling properties were different in and above the convective layer (Fischer et al. 2013).

The date and location of the simulation, 20 July 2007 over western France, were chosen to approximately match one of the flight tracks of the Convective and Orographically Induced Precipitation Study (COPS) field campaign considered in Fischer et al. (2013). The simulated weather situation at 1400 UT on that day (Fig. 1) shows a frontal band with intense precipitation over eastern France that is propagating to the east. In northern and western France, shallow to midlevel cumulus convection forms in the cold air that follows this front, with a cloud-top height of approximately 5 km. To perform the structure function analysis, we

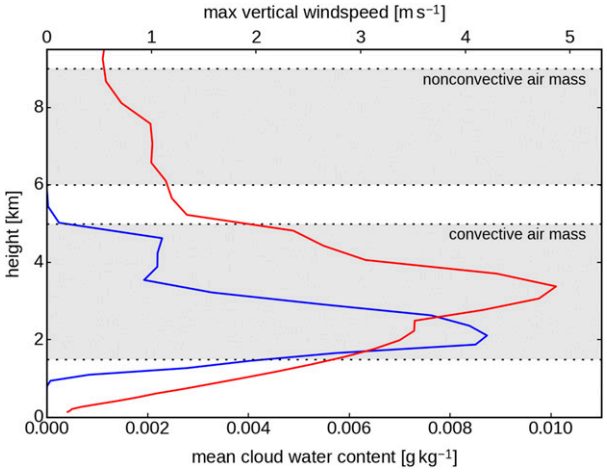

FIG. 2. Domain-averaged specific cloud water content (blue) and maximum vertical wind speed (red) with height. Shading indicates levels assigned to (bottom) the convective air mass and (top) the nonconvective air mass.

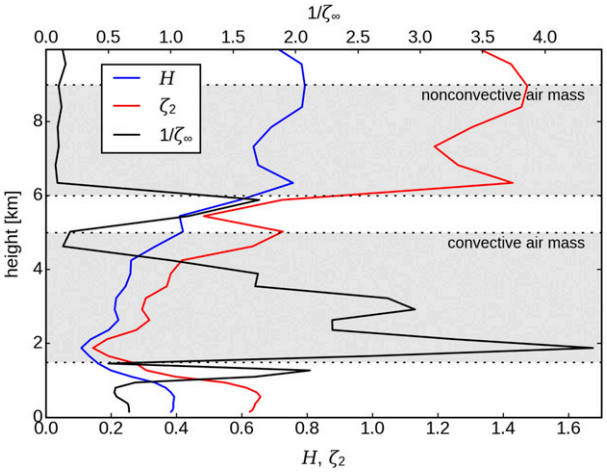

FIG. 3. Structure function scaling exponents H (blue) and ζ_2 (red) and intermittency $1/\zeta_\infty$ (black) with height. Shading indicates levels assigned to (bottom) the convective air mass and (top) the nonconvective air mass.

selected a west–east-oriented subdomain covering that region (solid box in Fig. 1). In the x direction the domain has a length of about 560 km, and in the y direction it consists of 51 grid points (143 km).

Figure 2 shows vertical profiles of the mean cloud water content q_c and maximum vertical wind w within this domain, further enabling us to distinguish between the air mass that is directly influenced by moist convection (where cloud water is present) and the air mass that is not. The plot shows that the maximum cloud-top height in the domain equals about 5.5 km. Most clouds, however, do not reach as high (3–5 km), leading to a continuous decrease in q_c. The maximum vertical wind peaks at a higher level than q_c but also shows a clear transition at about 5.5 km to a different regime. We thus define heights between 1.5 and 5 km as belonging to the "convective air mass" and assign heights between 6 and 9 km to the "nonconvective air mass" (as indicated in the figure).

The variations with height of the Hurst exponent H, the second-order scaling exponent ζ_2, and the intermittency $1/\zeta_\infty$ are plotted in Fig. 3, calculated from height-dependent structure functions. Note that only horizontal averaging of the increments was used [i.e., no sum over k in (3)]. All three variables also show a clear height dependence: away from the boundary layer the Hurst exponent H increases systematically with height, reaching a maximum at about 9 km. The minimum value can be found at 2 km, just above the boundary layer. The second-order scaling exponent ζ_2 behaves similarly; however, in contrast to H, a sharp transition to larger values can be found at the boundary between the convective and nonconvective air mass, which matches the transition in q_c and w described above.

The intermittency $1/\zeta_\infty$ shows an opposite height dependence, reaching a maximum of 4.4 at about 2 km and decreasing to very low values of about 0.1 above 6-km height. Again, its shape is clearly related to the cloud water and peak vertical wind profile of the domain (Fig. 2). There is, however, an exceptional spike just below 6 km, which is not seen in H and ζ_2. This spike coincides with strong gradients of H and ζ_2 at that level and a particularly bad fit of the scaling exponents to the function (6) (not shown).

The different character of the two air masses can be seen qualitatively in the humidity field. As an example, Fig. 4 shows two horizontal slices of the specific water vapor content q_v: one within the nonconvective air mass where the intermittency is low and one within the convective air mass with very high intermittency. The convective air mass is dominated by sharp spikes of high

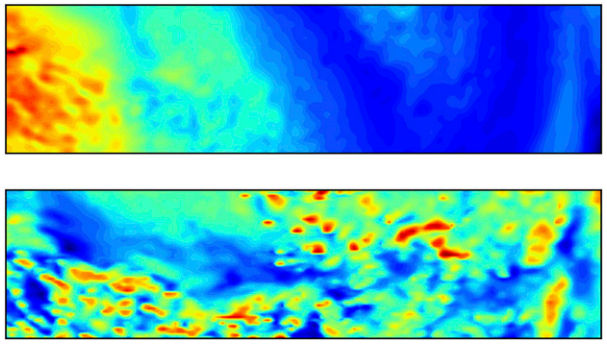

FIG. 4. Specific water vapor content q_v at (top) 6.8- and (bottom) 1.9-km heights for the region defined in Fig. 1. The top panel shows the nonconvective air mass and low intermittency ($1/\zeta_\infty = 0.08$). The bottom panel is part of the convective air mass and is located at the vertical intermittency maximum ($1/\zeta_\infty = 4.4$).

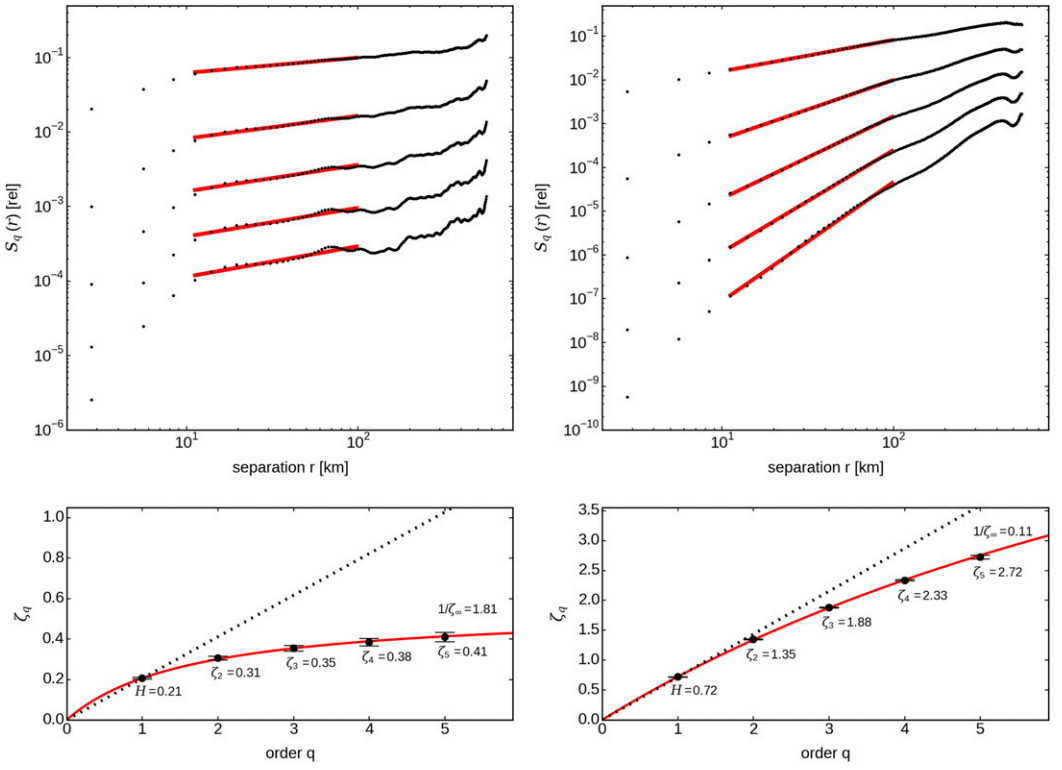

FIG. 5. (top) Structure functions up to the fifth order and (bottom) intermittency analysis of (left) the convective air mass and (right) the nonconvective air mass. In (top), the normalized q_v fields have been divided by 10 to better separate the structure functions of different orders in the plot. The first-order structure function is the topmost dotted line. The red lines show the result of the linear regression analysis in the range between 11 and 100 km according to (4). The slopes of the lines define the scaling exponents ζ_q, which are plotted in (bottom), together with their uncertainty estimation. The red lines in (bottom) show the fit of the scaling exponents to the scaling function (6) to determine the intermittency $1/\zeta_\infty$.

moisture, related to the convective updrafts. In the nonconvective air mass, however, the q_v field is much smoother with large-scale variability across the domain.

To get representative values of the scaling parameters for each of the two air masses as a whole, we computed the structure function again, this time also applying a vertical average to represent the ensemble mean. Before evaluating (3), the q_v field of each level has been normalized by the standard deviation of that level to reduce the effect of decreasing amplitudes of q_v with height. The resulting structure functions of each order for each air mass are plotted on a double-logarithmic scale in Fig. 5, together with the estimated linear regressions. The exponents (H and ζ_2–ζ_5) are plotted in the bottom panels, together with the estimated scaling function (6), from which the intermittency is derived. The resulting values for H, ζ_2, and $1/\zeta_\infty$ are also listed in Table 1. A comparison with Fig. 3 shows that the scaling properties of the two air masses computed in this way are roughly equal to the average of the height-dependent values over the respective range. The distinction between the two air masses is clearly visible in all scaling exponents but most pronounced in the intermittency.

The scaling exponents obtained by Fischer et al. (2013) using water vapor measurements from airborne lidar are given in the last column of Table 1 for comparison. The data combine three observation campaigns over Europe, Spitzbergen, and the western North Pacific and have been separated in a similar fashion into convective and nonconvective air masses based on cloud-top height. For the nonconvective air masses, there is good agreement of the scaling exponents and intermittency between simulation and measurements. In convective air masses, however, the values differ significantly, showing a much smaller intermittency and higher H and ζ_2 exponents in the observational data. Partly these differences can be explained by observational limitations and will be discussed in the following section.

b. *Sensitivity to observational limitations*

In this section, we use the numerical simulation as a surrogate data source to address the impact of three

TABLE 1. Scaling properties of water vapor. The first column of data lists the basic model output analysis as described in section 3a. The next three columns of data give the results of the sensitivity analyses of sections 3b(1)–3b(3), respectively. The last column recapitulates the results from Fischer et al. (2013).

		Model sensitivities			
	Model (basic analysis)	Doubled domain	Cloud mask	Single data series	Observation (three campaigns)
Convective air mass					
H	0.21	0.26	0.23	0.28 ± 0.09	0.35 ± 0.11
ζ_2	0.31	0.36	0.34	0.48 ± 0.17	0.65 ± 0.20
$1/\zeta_\infty$	1.81	1.83	1.62	0.85 ± 0.77	0.30 ± 0.16
Nonconvective air mass					
H	0.72	0.63	—	0.72 ± 0.08	0.63 ± 0.10
ζ_2	1.35	1.13	—	1.35 ± 0.16	1.19 ± 0.19
$1/\zeta_\infty$	0.11	0.19	—	0.09 ± 0.05	0.11 ± 0.09

intrinsic limitations of lidar observations on the structure function analysis: the domain size, data gaps caused by the presence of clouds, and the limited data sample of a single flight track.

1) DOMAIN SIZE

To check sensitivity of our results to the domain size, especially its length in the direction of the separation r (x direction), we repeat the analysis above using an extended domain. The domain size cannot, however, be chosen arbitrarily since the extent of the weather regime at hand is also limited. In our case, the region with the layer of convection extending up to about 5 km is bounded to the east by an intense squall line with very deep convection and to the west by a stratiform cloud regime over the ocean (Fig. 1). Within these boundaries it is possible to consider a domain that is doubled in the x direction, as indicated by the dotted box in Fig. 1. The scaling properties H, ζ_2, and $1/\zeta_\infty$ are computed as in section 3a, and the results are given in Table 1. It can be seen that the scaling parameters do not change significantly when the domain size is doubled. The small changes in the convective air mass do not appear to be systematic, since H and ζ_2 increase by about 20%, but the intermittency is essentially unchanged. The shifts in the nonconvective airmass parameters suggest a slight trend to a less smoothly varying air mass with a decrease of H and ζ_2 and an increase of $1/\zeta_\infty$.

2) DATA GAPS

Airborne lidar measurements of water vapor are impossible in the presence of optically thick clouds because of the absorption of the beam. As a result, a downward-pointing instrument mounted on an aircraft will obtain no data below clouds, leading to gaps in the data series. In past observational studies (Fischer et al. 2012, 2013), these gaps have been filled using linear interpolation before the structure function analysis was performed.

The influence of such data gaps and their padding by interpolation on the scaling exponents is now assessed by masking out values in the simulated data where a cloud is present at or above a grid point. Then, as in the observational analyses, water vapor values are linearly interpolated in the x direction to fill the gaps, and scaling exponents and intermittency are recomputed. This analysis was carried out for the convective air mass only since there are no clouds and thus no data gaps in the nonconvective air mass. The results are listed in Table 1 and show a slight decrease of the intermittency of about 10%, consistent with slight increases in H and ζ_2. This can be explained by the fact that clouds usually coexist with peaks in water vapor, and thus some of the q_v peaks that occur in or below clouds are smoothed out by the interpolation. However, compared to the scaling properties in the nonconvecting air mass, the change due to data gaps is small, and the distinction between the two air masses remains very clear.

3) SMALL SAMPLES

The lidar measurements provide a two-dimensional cross section of data through the observed air mass. A single flight segment thus represents a much smaller sample of the air mass than was used here for the analysis of the simulated humidity fields, where the structure function increments were averaged in the y direction over many sections. Note also that Fischer et al. (2012) and Fischer et al. (2013) did not use vertical averaging of the increments but averaged the resulting height-dependent scaling exponents and intermittency instead. As a result, the ensemble average of the increments was only represented by spatial averaging along the flight direction, and scaling properties were derived from single one-dimensional data series using (2). The consequences of this procedure are explored here by subsampling the simulated data in the same way.

When calculating scaling exponents and intermittency from single data series, noise and variability increase

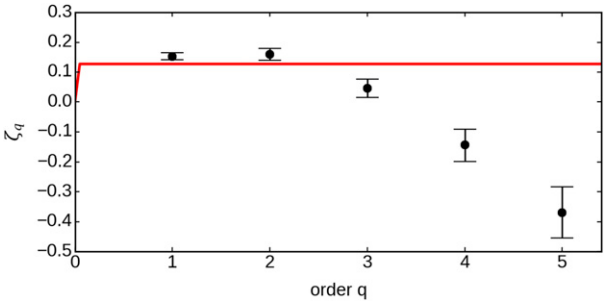

FIG. 6. Example for a bad fit of the scaling exponents (dots with error bars) to the scaling function (6) (red line). The scaling exponents are calculated from a single one-dimensional data series picked from the convective air mass.

and may result in bad power-law fits, bad fits of the scaling function (6), or both. Figure 6 shows an example for a bad fit of the scaling function from a selected $q_v(x)$ slice in the convective air mass. The large error bars of the scaling exponents also indicate large uncertainties and thus bad fits to the power law (4). The $q_v(x)$ series with particularly bad fits were found to be characterized by a decrease of the scaling exponents with higher orders, which cannot be represented by a function of the form (6).

In our previous observational study (Fischer et al. 2013), such data series have been discarded by requiring a coefficient of determination above 0.95 for the intermittency fit. For the present analysis, we will require that the mean coefficient of determination of the scaling exponents averaged over orders 1–5 is above 0.5 and that the average residual of the fit to the scaling function (6) is below 1σ. With these requirements, 55% of the data series in the convective air mass and 85% of the data series in the nonconvective air mass are considered ''valid'' and will be analyzed. The criteria are less strict than those used in the observational studies but they result in a similar fraction of valid data.

The mean values of the valid data sample for H, ζ_2, and $1/\zeta_\infty$ together with the standard deviations are listed in Table 1. In the nonconvective air mass, the values are almost exactly equal to those derived from the airmass-averaged increments in the first column. However, in the convective air mass there are larger differences. While the Hurst exponent is similar, the higher-order exponents differ increasingly, leading to a particularly large difference in the intermittency parameter $1/\zeta_\infty$. The reason for this discrepancy can be found in the exclusion of data series that do not meet the fit criteria defined above. Bad fits are highly correlated with very low high-order scaling exponents and large departures from monofractal behavior, as indicated by the example in Fig. 6. As a result, the resulting intermittency value is sensitive to the arbitrary choice of the fit criteria. Stricter criteria that exclude more data lead to lower intermittency, while more relaxed criteria that exclude less data lead to higher intermittency. These results indicate that the past structure function analyses of lidar observations very likely underestimated the intermittency in convective air masses, and the distinction between convective and nonconvective air masses may be more pronounced in reality.

4. Summary and discussion

Motivated by observational studies of multifractal scaling in tropospheric water vapor variability, the present study performs a horizontal structure function analysis of water vapor data from COSMO model simulations with a grid mesh size of 2.8 km. Power laws are identified up to the fifth order over horizontal spatial scales from 11 to 100 km. Based on cloud water content and vertical wind, the simulated dataset has been split into two air masses, a convective regime where cumulus clouds were active up to a height of about 5 km, and a nonconvective regime above the cloud-top height. The two regimes are found to be characterized by significantly different scaling exponents and intermittency values, with rough ($H = 0.21$) and highly intermittent structures ($1/\zeta_\infty = 1.81$) in the convective air mass and smooth ($H = 0.72$) and almost monofractal ($1/\zeta_\infty = 0.11$) behavior in the nonconvective air mass.

A comparison of the scaling statistics based on the COSMO simulation with the observational results from three flight campaigns showed that the distinction between convective and nonconvective air masses is robust and is reflected clearly in the scaling parameters considered. However, the exact values of the parameters differ in the convective air mass, and, in particular, the intermittency calculated from the model output is much higher than the values derived from observations. It should also be noted that not all weather regimes have been observed, and, in particular, lidar observations have not been carried out in the immediate vicinity of intense deep convection, which is often obscured by cirrus.

By resampling the model data in the same way as the observational analysis, it could be shown that two limitations of airborne lidar measurements systematically reduce the estimation of intermittency. First, data gaps below clouds and their padding by interpolation reduce spikes in the water vapor field that coincide with clouds and thus reduce intermittency. Second, bad fits in the estimation of the scaling exponents and especially the

intermittency occur preferentially in data series with low high-order scaling exponents and high intermittency. Rejection of such data series by some arbitrarily specified fit quality criterion is thus problematic since it systematically shifts the parameters toward nonintermittent monofractal behavior. Indeed, when considering these limitations in the evaluation of the simulated data, we found an intermittency value that was much closer to the values reported in the observational study of Fischer et al. (2013).

The true value of intermittency in the convective air mass remains uncertain from the results of our current study. The intermittency values from observations are likely too low, but the values determined from model output also suffer from limitations. While a resolution of 2.8 km is considered to be convection permitting in the sense that simulations produce better results than would be obtained using a convective parameterization, the details of the convective motions and resulting water vapor variability are not resolved. Especially for the shallow to midlevel convection considered here, the resolution might still be coarse, and future studies with higher resolution may result in different scaling exponents and intermittency.

Despite these uncertainties in the exact quantification of the intermittency, the numerical model succeeded in reproducing the observed differences in scaling behavior between convective and nonconvective air masses. This suggests that simulations at convective-permitting resolution can be a valuable tool for analyzing the physical mechanisms responsible for the variability of water vapor in the atmosphere and its regime dependence. Furthermore, the compact characterization of variability that the structure functions provide on scales that are subgrid for many global models may be useful in the development of parameterizations of moist processes. For example, in the stochastic convective parameterization of Plant and Craig (2008), an ensemble of convective plumes is launched within a single model grid box. At present, the environmental air entrained by all plumes is assumed to have larger-scale mean properties, but in reality each plume should entrain air drawn from the distribution of subgrid humidity. This will likely increase the variability of the convective ensemble and may lead to significantly different behavior for convection initiated in a previously undisturbed air mass in comparison to a region where convection is ongoing because of the different humidity distributions.

Acknowledgments. This work was funded by the German Science Foundation (DFG) through the Priority Program SPP-1294 "High Altitude and Long Range Research Aircraft" (HALO) and the Transregional Collaborative Research Center SFB/TRR 165 "Waves to Weather" (within the subproject "Upscale impact of diabatic processes from convective to near-hemispheric scale"). The observational dataset used in this work arises from the DLR Falcon participation in COPS/ETReC, which was supported by the DFG as part of SPP-1167 "Quantitative Precipitation Forecast." During T-PARC, the DLR Falcon aircraft was sponsored by an international consortium from Germany, the United States, Japan, South Korea, and Canada.

REFERENCES

Baldauf, M., A. Seifert, J. Förstner, D. Majewski, M. Raschendorfer, and T. Reinhardt, 2011: Operational convective-scale numerical weather prediction with the COSMO model: Description and sensitivities. *Mon. Wea. Rev.*, **139**, 3887–3905, doi:10.1175/MWR-D-10-05013.1.

Bierdel, L., P. Friederichs, and S. Bentzien, 2012: Spatial kinetic energy spectra in the convection-permitting limited-area NWP model COSMO-DE. *Meteor. Z.*, **21**, 245–258, doi:10.1127/0941-2948/2012/0319.

Brethouwer, G., and E. Lindborg, 2008: Passive scalars in stratified turbulence. *Geophys. Res. Lett.*, **35**, L06809, doi:10.1029/2007GL032906.

Calif, R., and F. G. Schmitt, 2012: Modeling of atmospheric wind speed sequence using a lognormal continuous stochastic equation. *J. Wind Eng. Ind. Aerodyn.*, **109**, 1–8, doi:10.1016/j.jweia.2012.06.002.

Cho, J. Y. N., and Coauthors, 1999: Horizontal wavenumber spectra of winds, temperature, and trace gases during the pacific exploratory missions: 1. Climatology. *J. Geophys. Res.*, **104**, 5697–5716, doi:10.1029/98JD01825.

——, R. E. Newell, and G. W. Sachse, 2000: Anomalous scaling of mesoscale tropospheric humidity fluctuations. *Geophys. Res. Lett.*, **27**, 377–380, doi:10.1029/1999GL010846.

Cusack, S., J. M. Edwards, and R. Kershaw, 1999: Estimating the subgrid variance of saturation, and its parameterization for use in a GCM cloud scheme. *Quart. J. Roy. Meteor. Soc.*, **125**, 3057–3076, doi:10.1002/qj.49712556013.

Fang, X., and Y.-H. Kuo, 2015: A new generic method for quantifying the scale predictability of the fractal atmosphere: Applications to model verification. *J. Atmos. Sci.*, **72**, 1667–1688, doi:10.1175/JAS-D-14-0112.1.

Fischer, L., C. Kiemle, and G. C. Craig, 2012: Height-resolved variability of midlatitude tropospheric water vapor measured by airborne lidar. *Geophys. Res. Lett.*, **39**, L06803, doi:10.1029/2011GL050621.

——, G. C. Craig, and C. Kiemle, 2013: Horizontal structure function and vertical correlation analysis of mesoscale water vapor variability observed by airborne lidar. *J. Geophys. Res. Atmos.*, **118**, 7579–7590, doi:10.1002/jgrd.50588.

Hamilton, K., Y. O. Takahashi, and W. Ohfuchi, 2008: Mesoscale spectrum of atmospheric motions investigated in a very fine resolution global general circulation model. *J. Geophys. Res.*, **113**, D18110, doi:10.1029/2008JD009785.

Kahn, B. H., and J. Teixeira, 2009: A global climatology of temperature and water vapor variance scaling from the atmospheric infrared sounder. *J. Climate*, **22**, 5558–5576, doi:10.1175/2009JCLI2934.1.

——, and Coauthors, 2011: Temperature and water vapor variance scaling in global models: Comparisons to satellite and aircraft data. *J. Atmos. Sci.*, **68**, 2156–2168, doi:10.1175/2011JAS3737.1.

Lewis, G. M., P. H. Austin, and M. Szczodrak, 2004: Spatial statistics of marine boundary layer clouds. *J. Geophys. Res.*, **109**, D04104, doi:10.129/2003JD003742.

Lovejoy, S., A. Tuck, and D. Schertzer, 2010: Horizontal cascade structure of atmospheric fields determined from aircraft data. *J. Geophys. Res.*, **115**, D13105, doi:10.1029/2009JD013353.

Marshak, A., A. Davis, W. Wiscombe, and R. Cahalan, 1997: Scale invariance in liquid water distributions in marine stratocumulus. Part II: Multifractal properties and intermittency issues. *J. Atmos. Sci.*, **54**, 1423–1444, doi:10.1175/1520-0469(1997)054<1423:SIILWD>2.0.CO;2.

Nastrom, G. D., W. H. Jasperson, and K. S. Gage, 1986: Horizontal spectra of atmospheric tracers measured during the global atmospheric sampling program. *J. Geophys. Res.*, **91**, 13 201–13 209, doi:10.1029/JD091iD12p13201.

Pierrehumbert, R. T., 1996: Anomalous scaling of high cloud variability in the tropical Pacific. *Geophys. Res. Lett.*, **23**, 1095–1098, doi:10.1029/96GL01121.

Plant, R., and G. C. Craig, 2008: A stochastic parameterization for deep convection based on equilibrium statistics. *J. Atmos. Sci.*, **65**, 87–105, doi:10.1175/2007JAS2263.1.

Pressel, K. G., and W. D. Collins, 2012: First-order structure function analysis of statistical scale invariance in the AIRS-observed water vapor field. *J. Climate*, **25**, 5538–5555, doi:10.1175/JCLI-D-11-00374.1.

——, ——, and A. R. Desai, 2010: Variance scaling in water vapor measurements from a tall tower. *13th Conf. on Cloud Physics*, Portland, OR, Amer. Meteor. Soc., P1.77. [Available online at https://ams.confex.com/ams/13CldPhy13AtRad/webprogram/Paper171839.html.]

——, ——, and ——, 2014: The spatial scale dependence of water vapor variability inferred from observations from a very tall tower. *J. Geophys. Res. Atmos.*, **119**, 9822–9837, doi:10.1002/2013JD021141.

Schemann, V., B. Stevens, V. Grtzun, and J. Quaas, 2013: Scale dependency of total water variance, and its implication for cloud parameterizations. *J. Atmos. Sci.*, **70**, 3615–3630, doi:10.1175/JAS-D-13-09.1.

Selz, T., and G. Craig, 2015: Upscale error growth in a high-resolution simulation of a summertime weather event over Europe. *Mon. Wea. Rev.*, **143**, 813–827, doi:10.1175/MWR-D-14-00140.1.

Shraiman, B. I., and E. D. Siggia, 2000: Scalar turbulence. *Nature*, **405**, 639–646, doi:10.1038/35015000.

Skamarock, W. C., 2004: Evaluating mesoscale NWP models using kinetic energy spectra. *Mon. Wea. Rev.*, **132**, 3019–3032, doi:10.1175/MWR2830.1.

Stevens, B., and S. Bony, 2013a: Water in the atmosphere. *Phys. Today*, **66**, 29–34, doi:10.1063/PT.3.2009.

——, and ——, 2013b: What are climate models missing? *Science*, **340**, 1053–1054, doi:10.1126/science.1237554.

Tiedtke, M., 1989: A comprehensive mass flux scheme for cumulus parameterization in large-scale models. *Mon. Wea. Rev.*, **117**, 1779–1800, doi:10.1175/1520-0493(1989)117<1779:ACMFSF>2.0.CO;2.

Tjemkes, S., and M. Visser, 1994: Horizontal variability of temperature, specific humidity, and cloud liquid water as derived from spaceborne observations. *J. Geophys. Res.*, **99**, 23 089–23 105, doi:10.1029/94JD01718.

Tompkins, A. M., 2002: A prognostic parameterization for the subgrid-scale variability of water vapor and clouds in large-scale models and its use to diagnose cloud cover. *J. Atmos. Sci.*, **59**, 1917–1942, doi:10.1175/1520-0469(2002)059<1917:APPFTS>2.0.CO;2.

Tuck, A. F., S. J. Hovde, E. C. Richard, D. W. Fahey, R. S. Gao, and T. P. Bui, 2003: A scaling analysis of ER-2 data in the inner vortex during January–March 2000. *J. Geophys. Res.*, **107**, 8306, doi:10.1029/2001JD000879.

Wang, H., G. Feingold, R. Wood, and J. Kazil, 2010: Modelling microphysical and meteorological controls on precipitation and cloud cellular structures in Southeast Pacific stratocumulus. *Atmos. Chem. Phys.*, **10**, 6347–6362, doi:10.5194/acp-10-6347-2010.

Yokohata, T., S. Emori, T. Nozawa, Y. Tsushima, T. Ogura, and M. Kimoto, 2005: Climate response to volcanic forcing: Validation of climate sensitivity of a coupled atmosphere–ocean general circulation model. *Geophys. Res. Lett.*, **32**, L21710, doi:10.1029/2005GL023542.

Zhang, M., 2013: Cloud–climate feedback: How much do we know? *Observation, Theory and Modeling of Atmospheric Variability*, X. Zhu et al., Eds., World Scientific Series on Asia-Pacific Weather and Climate, Vol. 3, World Scientific Publishing Co., 161–183.